Available online at www.sciencedirect.com
ScienceDirect
Medical Engineering & Physics 30 (2008) 123–133
Medical Engineering & Physics
www.elsevier.com/locate/medengphy

Technical note

Use of multiple wearable inertial sensors in upper limb motion tracking

Huiyu Zhou[a], Thomas Stone[b], Huosheng Hu[c,*], Nigel Harris[b]

[a] *Department of Electronic Engineering, Queen Mary, University of London, Mile End Road, London N1 4NS, UK*
[b] *School for Health, University of Bath, Bath BA1 1RL, UK*
[c] *Department of Computer Science, University of Essex, Colchester CO4 3SQ, UK*

Received 14 July 2006; received in revised form 17 November 2006; accepted 19 November 2006

Abstract

This paper presents a new human motion tracking system using two wearable inertial sensors that are placed near the wrist and elbow joints of the upper limb. Each inertial sensor consists of a tri-axial accelerometer, a tri-axial gyroscope and a tri-axial magnetometer. The turning rates of the gyroscope were utilised for localising the wrist and elbow joints on the assumption that the two upper limb segment lengths are known a priori. To determine the translation and rotation of the shoulder joint, an equality-constrained optimisation technique is adopted to find an optimal solution, incorporating measurements from the tri-axial accelerometer and gyroscope. Experimental results demonstrate that this new system, compared to an optical motion tracker, has RMS position errors that are normally less than 0.01 m, and RMS angle errors that are 2.5–4.8°.

Keywords: Motion tracking; Upper limb; Rehabilitation; Inertial sensor; Optimisation

1. Introduction

Stroke is the biggest cause of disability in the UK. About 110,000 people each year experience a first stroke, and a further 30,000 have a further stroke. More than 75% of these people require multi-disciplinary assessments and appropriate rehabilitative treatments after they are discharged from the hospital [1,2]. This places a large demand on community healthcare services, which often have quite limited therapy resources. As a result, there is considerable interest in training aids or intelligent systems that, as complementary tools, can support rehabilitation in the patient's home rather than in hospital [3].

One of the goals of stroke rehabilitation is to enable a stroke patient to regain the highest possible level of motor function. Although some motor function may return subsequent to a stroke, recovery is an ongoing process and it is known that rehabilitative strategies can improve the recovery of functional movement [4]. There remains a dearth of instrumented assessment equipment appropriate for use at home that can augment and evaluate current rehabilitative interventions [5]. The availability of this equipment, which could be used at home with greater frequency and for a longer period of time, may be a multi-disciplinary model and a more cost-effective approach to deliver post-stroke rehabilitation services [6].

Devices that can accurately track the position of the body in space are an important component of such a rehabilitative system. Using these devices, trajectories of human movements can be immediately recovered. Physiotherapists in hospitals can remotely "observe" the human movements via networking and then instruct the patients for the following recovery process. Currently, these devices made motion detection feasible by using inertial, magnetic, mechanical, or visual sensors, etc. Next, we summarise the characteristics of the existing sensor based systems.

Inertial sensors were first used in the detection of human movements in the 1950s [7]. However, these sensors were not commercially available until, in recent years, their

* Corresponding author. Tel: +44 1206 872297; fax: +44 1206 872788.
E-mail address: hhu@essex.ac.uk (H. Hu).

1350-4533/$ – see front matter © 2007 IPEM. Published by Elsevier Ltd. All rights reserved.
doi:10.1016/j.medengphy.2006.11.010

performance had been dramatically improved. Since inertial sensors are sourceless, compact and light, they have been a popular choice for applications such as motion tracking, human–computer interface, and animation. For example, Veltink et al. [8] investigated the difference between static and dynamic activities using uniaxial accelerometers. Similar techniques have also been reported in Boonstra et al. [9], Lyons et al. [10], Mayagoitia et al. [11], Naja. et al. [12]. Although these approaches were successful in their particular applications, they are extremely problem-specific and some seriously suffered from the drift problem. These problems negatively affect the application of inertial sensors in a poorly controlled environment (e.g. homes).

As a possible solution, robotics or mechatronics (i.e. MIT-MANUS by Krebs et al. [13]) have been explored due to their stable and reliable performance. These robotic systems utilised potentiometers or gyroscopes to estimate limb rotation. Other sensors such as CCD cameras can be integrated within an inertial based system so as to mitigate drifts [14]. Kalman filters have been used for the purpose of sensor fusion [15]. Many of these systems are complex to set-up with intensive computation and are not suitable for a home environment [16].

To develop a home based rehabilitation system, our main intention in this paper was to design a motion detector using body-mounted inertial sensors, which is able to provide measurements of upper limb motion (the work developed can easily be extended to the case of lower limb motion detection). Kinematic models using two commercially available sensors were first designed. This configuration allowed us to recover the position of the wrist and elbow joints. To estimate the position of the shoulder joint, a Lagrangian based optimisation technique was then presented, which integrated the values of acceleration and the estimated value of rotation measured from both the inertial sensors. The novelty of this study is that a new motion detection strategy was proposed, where the position of three joints on the human arm could be obtained only deploying two inertial sensors. Each inertial sensor consists of a tri-axial accelerometer, a tri-axial gyroscope and a tri-axial magnetometer. This feature made our system different from the classical devices, which normally demanded more sensors to reach the same goal.

2. Methods

2.1. General

Since we are interested in tracking a human arm, we use a skeleton structure with two segments linked by a revolute joint. Only the position of the wrist (in the middle between the radial and ulnar styloid processes), elbow (lying anterior to the olecranon process) and shoulder joints (the centre of the humeral head) were calculated. The arm movements were sampled using two commercially available MT9B inertial sensors (Xsens, The Netherlands), placed on the two segments, respectively. The whole motion tracking system (see Fig. 1) was implemented in the environment of Visual Studio C++, where the computer is a Media PC with a VIA Nehemiah/1.2 GHz CPU.

Measurements from the proposed tracking system were compared to the ground-truthed data from: (1) the designed paths for a subject's arm to follow (detailed in a later section), and (2) an optical motion tracker, CODA (Charnwood Dynamic Ltd., UK), which as a reference provided absolute position of the moving arm. For system comparison, the coordinate system of the proposed tracker can be aligned with that of the reference data using a direct 3D coordinate transformation. To relate the movements of the sensor to those of the segments, a sensor calibration needs to be conducted [17]. Errors in motion estimation can be presented using the mean, standard deviation, and root of the mean of the squared errors (RMS). Additionally, correlation coefficients and non-parametric tests (Wilcoxon sign rank tests) were used for evaluating the similarity between the outcomes of our system and the CODA system.

2.2. Estimation of the joint position

The flowchart of the dynamic estimation is illustrated in Fig. 2. The raw acceleration signals were low-passed filtered (cut-off frequency: 10 Hz) to remove high-frequency noise, while the raw gyroscopic signals were high-pass filtered (cut-off frequency: 0.05 Hz) to reduce the internal drift. To determine the position of an arm in a world (global) coordinate system, we need to transform the inertial measurements from the sensor coordinate system to the world (global) coordinate system.

Consider a rigid body moving in the earth frame. The world frame is w, and the sensor body frame is b. $\mathbf{R}_b^w$, a 3×3 rotation matrix, indicates the orientation transformation from the b-frame to the w-frame:

$$\mathbf{v}^w = \mathbf{R}_b^w \mathbf{v}^b, \tag{1}$$

where $\mathbf{v}^w$ and $\mathbf{v}^b$ represent the linear velocity vector of the sensor in the w- and b-frames, respectively. The state of $\mathbf{R}_b^w$ at the next instant, $\mathbf{R}_b^{w'}$, can be updated as follows:

$$\dot{\mathbf{R}}_b^w = \mathbf{R}_b^w S(\boldsymbol{\omega}^b), \tag{2}$$

where $S(\boldsymbol{\omega}^b) \equiv [\boldsymbol{\omega}^b \times]$ is the skew-symmetric matrix that is formed using the cross-product operation of the angular velocity estimates $\boldsymbol{\omega}^b$ [18, p. 141]. In fact, the new rotation matrix $\mathbf{R}_b^{w'}$ will be equivalent to the previous $\mathbf{R}_b^w$ plus $\dot{\mathbf{R}}_b^w$ multiplied by a time interval (1/25 s herewith). Once the rotation matrix has been obtained, then the acceleration readings in the w-frame will be deduced as

$$\mathbf{a}^w = \mathbf{R}_b^w \mathbf{a}^b + \mathbf{G}^w, \tag{3}$$

where $\mathbf{G}^w = [0, 0, 9.81]^{\mathrm{T}}\,\mathrm{m\,s^{-2}}$ is the local gravity vector whose effect on the acceleration needs to be eliminated. Euler angles can be estimated using a strapdown integration method

Fig. 1. Illustration of the designed tracking system.

reported in Luinge [15]. In this study, we used Euler angles rather than quaternion to represent the angular changes as the latter demands a non-linear and intensive computation.

Once having the representation of accelerations and Euler angles in the world frame, we can locate the position of the wrist and elbow joints in the world frame using the estimated Euler angles. Before this computation starts, let us assume that the length of the lower arm (ulna styloid to olecranon process) is L_1, and the length of the upper arm (olecranon process to acromian process) is L_2. In the static state, the x-axis of these two inertial sensors was collinear with the direction of the upper and lower arm. During dynamic movements, the elbow position $\mathbf{P}_e$ in the shoulder-originated coordinate system was calculated as

$$\mathbf{P}_e = \mathbf{R}_{es}\mathbf{P}_{e_0}, \tag{4}$$

where $\mathbf{R}_{es}$ is the rotation matrix of the upper arm, and $\mathbf{P}_{e_0} = [L_1, 0, 0]^{\mathrm{T}}$. Based on the estimation of the elbow position, the wrist position $\mathbf{P}_w$ in the shoulder-originated coordinate system was deduced as

$$\mathbf{P}_w = \mathbf{R}_{we}\mathbf{P}_{w_0} + \mathbf{P}_e, \tag{5}$$

where $\mathbf{R}_{we}$ is the rotation matrix of the lower arm (the origin is the elbow joint), and $\mathbf{P}_{w_0} = [L_2, 0, 0]^{\mathrm{T}}$.

The position of the shoulder joint was also computed as this is an important outcome measure during upper limb rehabilitation. We assume that total displacements of the wrist (or elbow) joint result from the combination of the pure translation of the shoulder joint and the pure rotation of the forearm and upper arm. The rotation component was calculated using the gyroscope signals. The translation component can be estimated using the acceleration measurements from both MT9B sensors. By double-integrating these accelerations, an over-determined solution for the translation component of the shoulder joint was generated. However, this solution results in significant drifts due to sensor noise or offsets. To maximally suppress the potential drifts, a Lagrangian based optimisation technique was envisaged, where the rotation and translation components of the shoulder joint were combined with the length-constraint of each segment. This expectedly reduces drifts buried in the estimated displacements of the shoulder joint.

Let $\mathbf{D}_w$ be the displacement vector of the wrist joint only due to the angular variations of the lower arm (the elbow joint is the pivot of this rotation), and $\mathbf{P}_s$ the displacement vector of the shoulder joint only using the accelerations from the sensor placed on the upper arm. There exists two constraints as follows:

$$\int_0^{t_1}\int_0^{t_2} \mathbf{a}_e \,\mathrm{d}t - \mathbf{P}_e - \mathbf{P}_s \to 0 \tag{6}$$

and

$$\int_0^{t_1}\int_0^{t_2} \mathbf{a}_w \,\mathrm{d}t - \int_0^{t_1}\int_0^{t_2} \mathbf{a}_e \,\mathrm{d}t - \mathbf{D}_w \to 0, \tag{7}$$

where $\mathbf{a}_w$ and $\mathbf{a}_e$ represent the acceleration vectors of the two sensors placed on the lower and upper arms, respectively. t_1 and t_2 are two time instants.

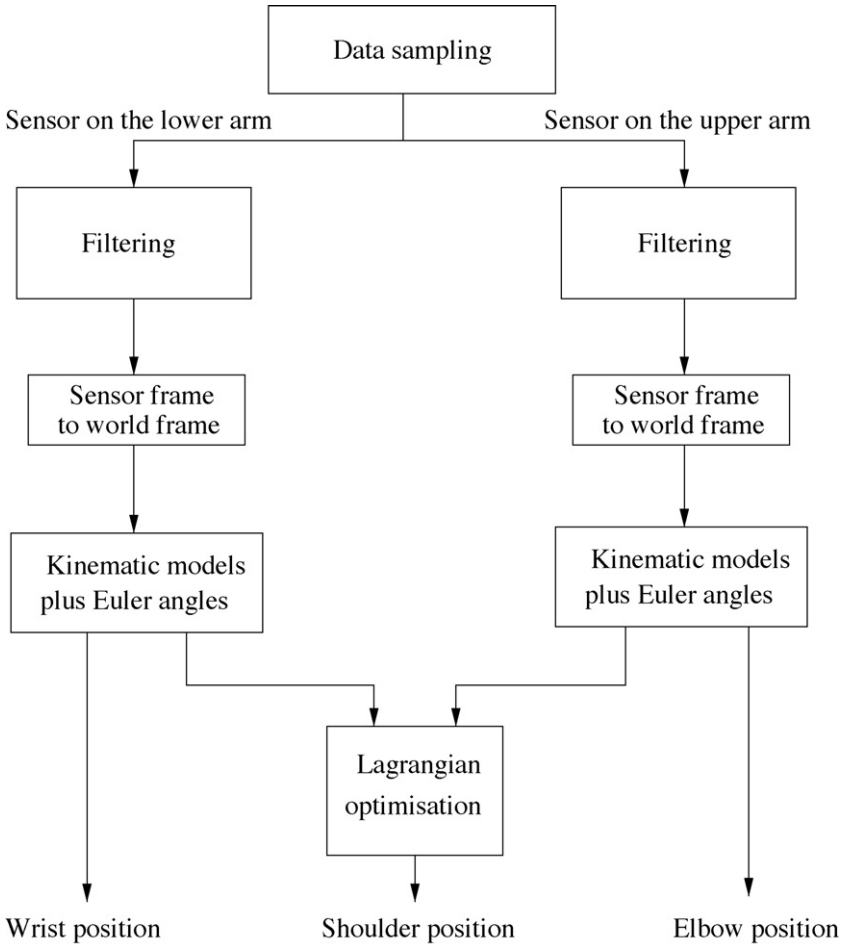

Fig. 2. Illustration of estimating the joint position during trajectory.

The determination of $\mathbf{P}_s$ can be treated as an equality-constrained optimisation problem, which is described as

$$L(t, \lambda) = \mathbf{S}_a - \lambda^{\mathrm{T}} \mathbf{S}_b, \tag{8}$$

where $\mathbf{S}_a = \int_0^{t_1} \int_0^{t_2} \mathbf{a}_e \, \mathrm{d}t - \mathbf{P}_e - \mathbf{P}_s$, and $\mathbf{S}_b = \int_0^{t_1} \int_0^{t_2} \mathbf{a}_w \, \mathrm{d}t - \int_0^{t_1} \int_0^{t_2} \mathbf{a}_e \, \mathrm{d}t - \mathbf{D}_w$. λ is a Lagrange-like multiplier and a diagonal matrix with diag[λ_{11}, λ_{22}, λ_{33}]. $\mathbf{P}_s$ can be derived if $L(t, \lambda)$ is minimised.

Using the Karush–Kuhn–Tucker (KKT) condition, we have

$$\frac{\partial L(t, \lambda)}{\partial t} = \frac{\partial \mathbf{S}_a}{\partial t} - \lambda^{\mathrm{T}} \frac{\partial \mathbf{S}_b}{\partial t} = 0, \tag{9}$$

where λ can be deduced if $\partial \mathbf{P}_s / \partial t$ is a constant. To obtain such a constant, in a pre-calibration stage, we kept the shoulder still during repeated movements (20 times), and then used a polynomial regression technique [19] to estimate λ via Eq. (9). In a home-based environment, the sensor kit will be placed on an upper limb of a healthy adult before it is applied to any stroke patient. This subject will be asked to keep his/her shoulder still during the required sampling so as to deduce a proper λ. In theory, λ is dependent on $\mathbf{S}_a$ and $\mathbf{S}_b$, which are only determined by the arm length. Sensor positions on arms do not affect the computation of λ unless the rigidness of the arm movements cannot be met.

After λ had been available, we were able to render $\mathbf{P}_s$ when the left side of Eq. (8) was minimized [20], while the shoulder moved during the data sampling.

2.3. Experimental set-up

Motivated by the evaluation methods described in Section 2.1, two experimental environments were set-up individually: one was with the designed paths, and the other was with the CODA tracker.

2.3.1. The "designed paths" experiment

By using Velcro straps, one of the MT9B sensors was attached to the upper arm with 2-cm distance to the elbow joint, and the other was tied with the lower arm with 2-cm distance to the wrist joint. These sensors faced outwards the arm. Four healthy male adults (20–40 years old) participated in this experiment. They started performing arm movements after being given simple instructions of where and how to move their arms. Two motion patterns were carefully designed and printed on two white paper, respectively. The

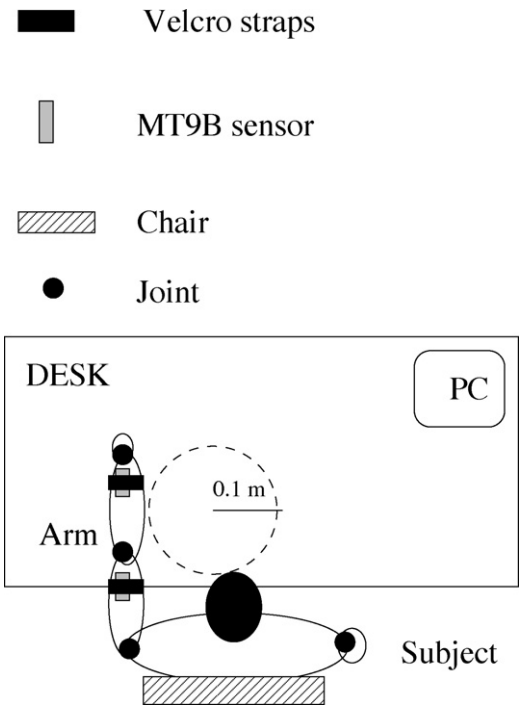

Fig. 3. Set-up in the "designed paths" experiment.

first is a circle (radius: 0.1 m), and the second is a rectangle (0.2 m×0.14 m). These parameters were chosen so that the subjects could freely and comfortably change their arm posture during the movements. The subjects (one-by-one) sat still in a solid chair with the pattern paper placed on a desk (height: 0.75 m) in front of them (Fig. 3). For the proposed tracking system, data was collected using the sample rate of 25 Hz.

2.3.2. The "optical tracker" experiment

Subjects sat in a chair in front of the CODA system while permitting their left arms to conduct specified movements in the viewing direction of the cameras on the CODA system (Fig. 4). The CODA system sampled with a rate of 200 Hz, and the data later can be re-sampled at 25 Hz for comparison to the outcomes of the proposed motion detector. This re-sampling possibly cause small details (or high-frequency components) in the measurements of the CODA system to be lost; however, it does not affect our measurements as the human movements in our experiments were not fast (≤12 Hz).

One MT9B sensor was placed as close to the wrist centre as possible on the palmer aspect (PA). The second MT9B sensor was placed on the lateral aspect of the upper arm on the line between the lateral epicondyle and the Acromian process (AP) (5 cm from the AP). Six CODA markers were placed on the following position for representing the upper limb's movements: (1) centre of the wrist midway between the ulner and radial styloid, (2) lateral epicondyle at the elbow, (3) AP, (4) trapezious, (5) T5 (spine of vertebrae), and (6) C7 (ventral ramus of root). Two wand markers were used to assess arm rotation: 5 cm wand was placed midway between the wrist

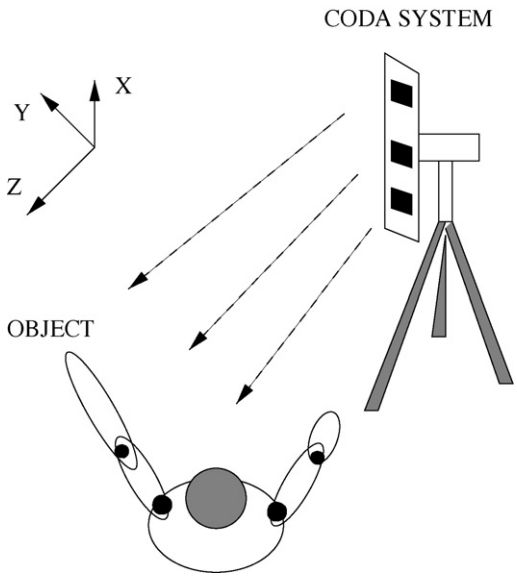

Fig. 4. Set-up in the "CODA optical tracker" experiment.

marker and the elbow. The second wand was placed midway between the elbow and the AP. Two reference markers were placed on the chair to define the vertical direction.

Three tests have been performed, which consist of target reaching, shoulder shrugging and forearm rotation. In the first experiment, the shoulder joint was fixed without moving. Theoretically, if the shoulder moves, the wrist and elbow positions will be under- or over-estimated. For the second experiment, the arm was naturally straight down before conducting the entire test. The forearm was rotated around the elbow joint in the third experiment.

3. Experimental results

For the purpose of clarity, the experimental results are shown in two parts: (1) the "designed paths" experiment, and (2) the "optical tracker" experiment.

3.1. The "designed paths" experiment

The experiment can be divided into two groups: (1) circular motion detection, and (2) square motion detection. For each group, we first present the Euler angles estimated from the two MT9B sensors using the proposed kinematic model. Then, we plot the position measurements against sample numbers. Finally, to discover the accuracy of the estimated position of the sensor mounted on the lower arm, we calculated the mean position for a period of 2 min, which was compared to the real shape of the designed path. The mean position of the sensor nearer the shoulder joint will also be presented but no expected value or ground-truth was available in our experiments. Fig. 5 illustrates the periodically changed tri-axial Euler angles for a subject in 40 s, estimated from the two sensors in the square motion. The tri-axial angle vari-

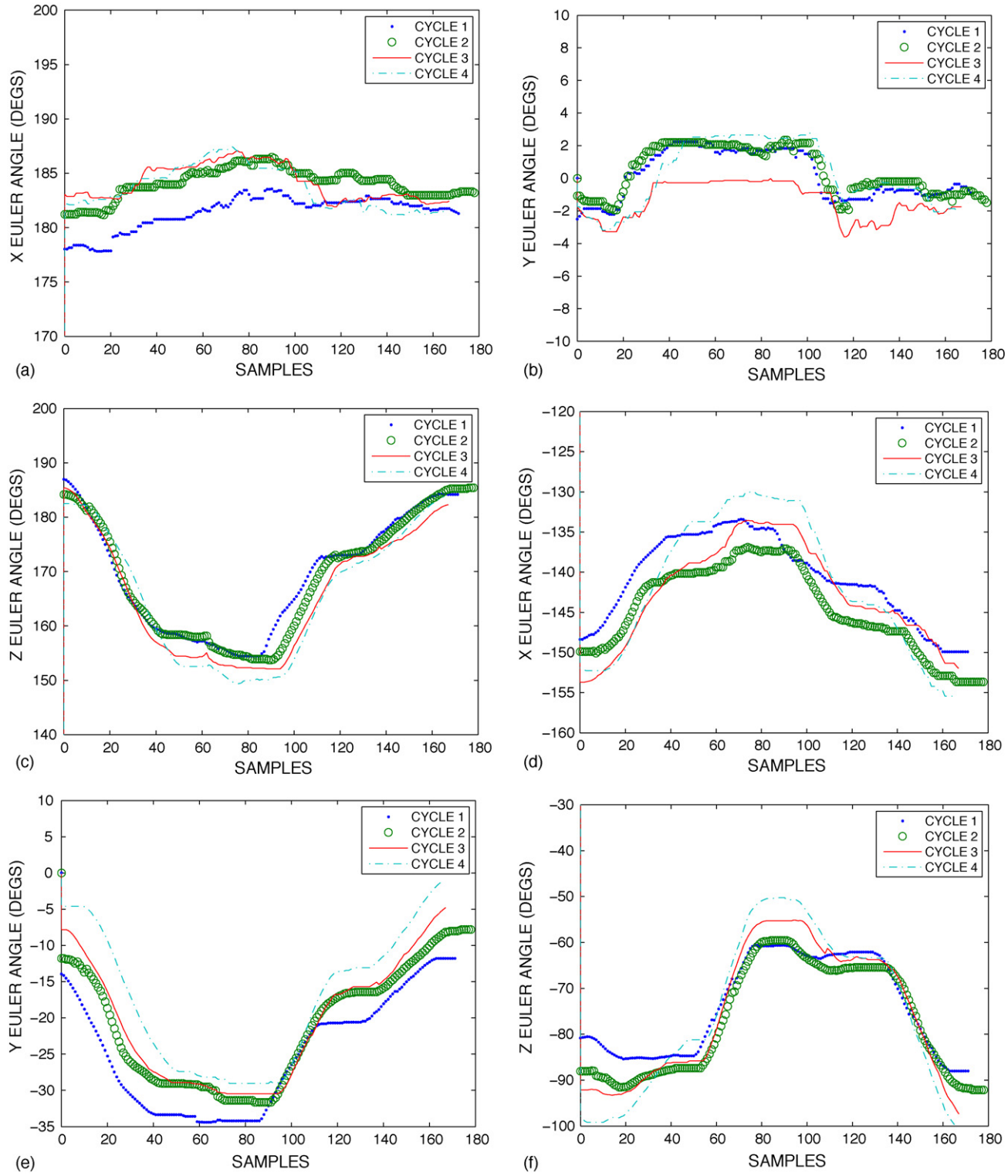

Fig. 5. Euler angle estimation of the two segments in square motion. (a) Lower arm: Euler angle (x); (b) lower arm: Euler angle (y); (c) lower arm: Euler angle (z); (d) upper arm: Euler angle (x); (e) upper arm: Euler angle (y); (f) upper arm: Euler angle (z).

ations are of 20°, 35°, and 50°(peak-to-peak), respectively. One can observe that the motion repetition had been stably recovered. As a result, the position estimation of the inertial sensors can be properly performed (see Fig. 6), where periodicity appears in the overall sub-figures. The circular motion has similar outcomes. We found that these errors were mainly due to the shaking arm, which did not exactly match the designed paths. For the position estimates from the all subjects,

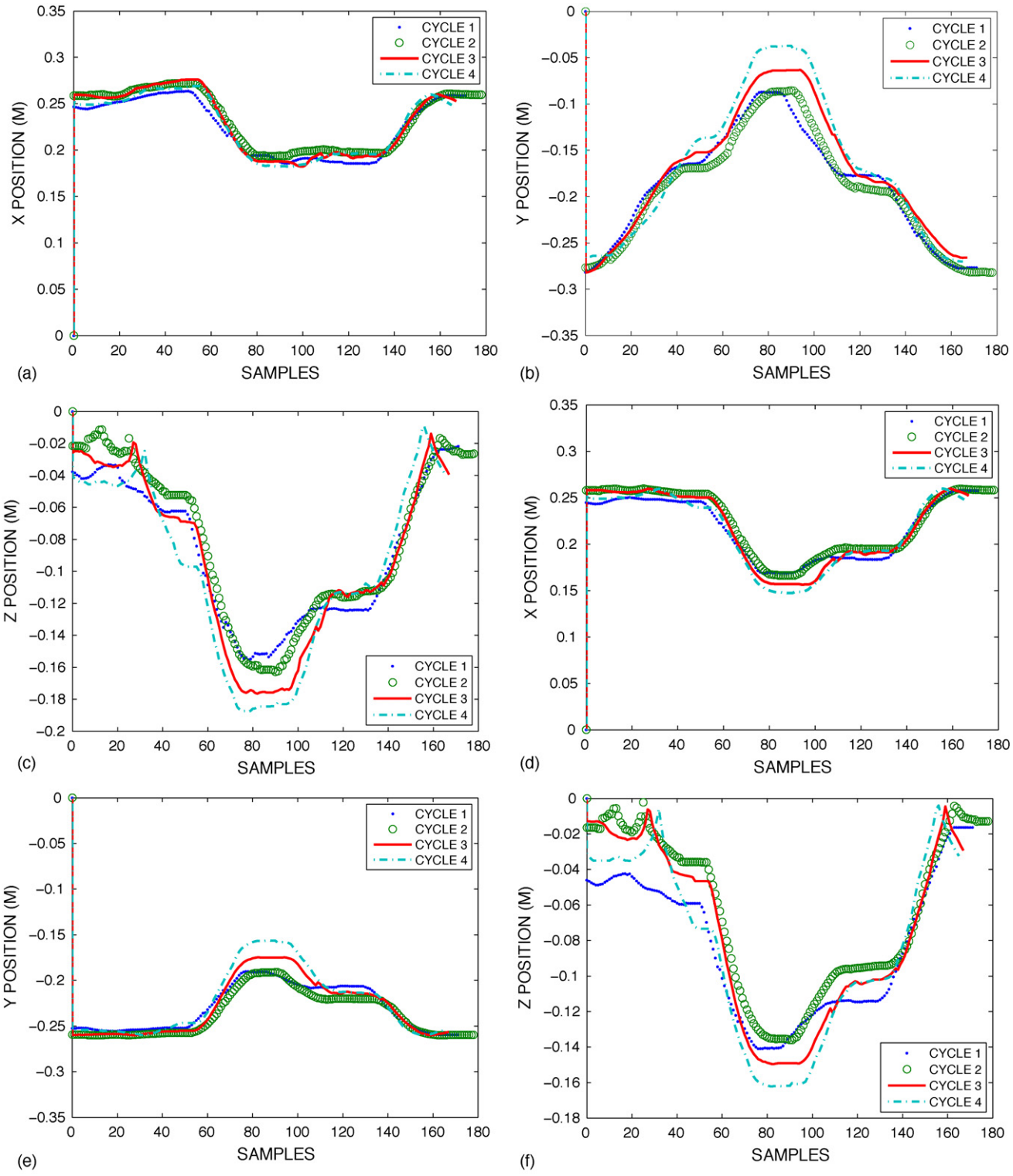

Fig. 6. Position estimation of the two joints in square motion. (a) Wrist: position (x); (b) wrist: position (y); (c) wrist: position (z); (d) elbow: position (x); (e) elbow: position (y); (f) elbow: position (z).

mean, standard deviation, and RMS errors are tabulated in Table 1.

We also investigate the consequence of placing two sensors at different positions on the arm. For example, both sensors were moved from their original position and away from their respective joints. Experimental results indicate that less than 0.5% averaging variations against 100 s arose from the sensor re-allocation.

Table 1
The wrist position (m) in the "designed paths" experiment

Location	Motion manners	Mean	S.D.	RMS	Correlation	*p*-Value
Wrist	Circular	0.006	0.014	0.015	0.96	0.48
	Square	0.004	0.011	0.012	0.98	0.56

3.2. The "optical tracker" experiment

Three tests have been conducted: reaching, shrugging and forearm rotation. The sample period is 20 s. Each subject was free to do individual tests with a normal speed. For the reaching test, the elbow flexion/extension angle is up to 100°. Fig. 7 illustrates example measurements of the wrist and elbow position in the reach test. This demonstrates that the measure-

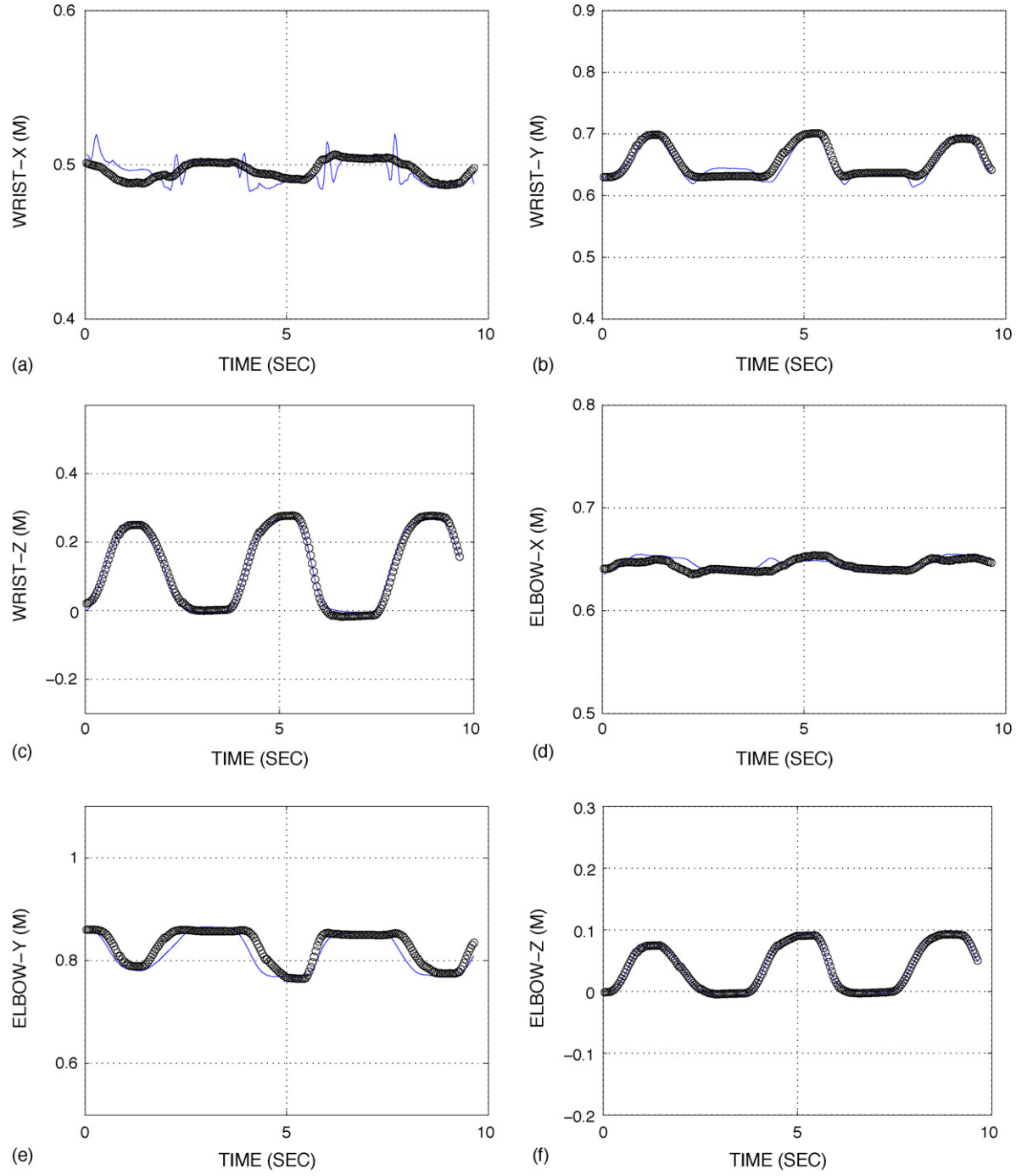

Fig. 7. (a–f) Example measurements of the wrist and elbow position in the reach test (circle lines, our system; solid lines, optical motion tracker).

Table 2
The wrist and elbow positions (m) in the "optical tracker" experiment

Test	Location	Mean	S.D.	RMS	Correlation	*p*-Value
Reaching	Wrist	0.003	0.006	0.007	0.98	0.31
	Elbow	0.006	0.009	0.01	0.97	0.43

Table 3
Elbow flexion/extension angles (°) in the "optical tracker" experiment

Test	Reaching
Mean	0.41
S.D.	2.34
RMS	2.41
Correlation	0.98
p-Value	0.44

ments by our method are accurate. The mean, standard deviation, and RMS with respect to the error residuals between the measurements of the CODA and our motion detectors have been shown in Table 2 (only the wrist and elbow positions are here provided). Since the measurements are tri-axial, we have calculated the mean values over the tri-axial estimates and only show these mean values in the table (and hereafter). Correlation coefficients and p values computed for the outcomes of these two systems are also shown in Table 2. These values can be used to show non-significance between the two data groups. In this application, we investigated each cycle (rather than the overall outcomes) of the periodic movements during the sample period. Meanwhile, statistical analysis of the estimated Euler angles are revealed in Table 3. From these two tables, it is evident that the proposed motion detector was effective due to the small RMS and large correlation coefficients.

For the shrugging test, the shoulder position changed with a displacement of 8 cm (approximately). Table 4 reveals very small errors in the estimation of the three joint positions. Similar to the reaching test, Table 5 shows the results of the forearm rotation test. It has been noticed that, although the proposed method has good performance in the angular estimation of the forearm (an example of the estimated Euler angle around the Z-axis is illustrated in Fig. 8), the statistic errors show that the mean and RMS values are larger than the estimated angles in the reaching test. Taking a closer look at these values, the errors might be due to the relative movements between the underlying bone and the sensors. The errors may also be due to the inertia of the gyroscopes. Compared to the latter problem, the former one is much easier to be solved if the sensor attachment is properly designed. For the time being, the sensors are attached to the arms using Velcro straps. The viable straps may lead to free motion of the sensors so a relatively rigid sensor attachment needs to be produced (see Section 4).

Table 5
Forearm rotation angles (°) in the "optical tracker" experiment

Test	Rotation
Mean	0.06
SD	4.82
RMS	4.83
Correlation	0.94
p-Value	0.35

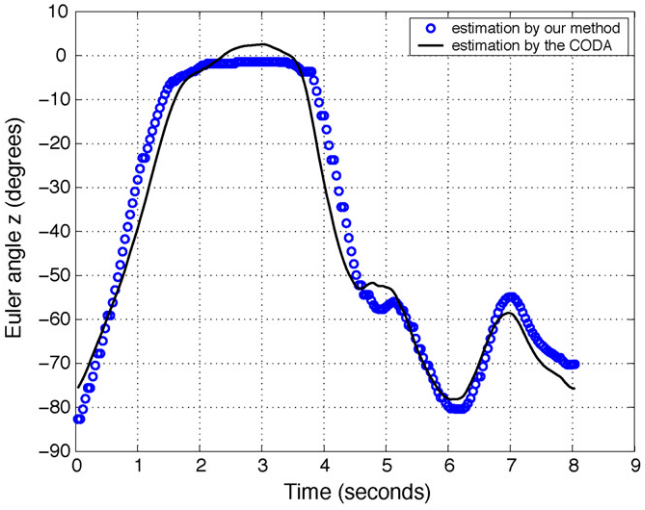

Fig. 8. An example of the estimated Euler angle z in the forearm rotation test.

4. Discussion

Our main contribution in this paper is the integration of accelerometers and gyroscopes, which has been fully justified in detection of upper limb movements. Literature shows that accelerometers have been used to objectively estimate body movements. These sensors were extremely valuable to discriminate between a static and dynamic segments or elements, e.g. a disabled human limb due to strokes. Following Veltink's work [8], Uiterwaal et al. [21] and Lyons et al. [10] used predetermined fixed threshold levels to define indi-

Table 4
The three joints' position (m) in the "optical tracker" experiment

Test	Location	Mean	S.D.	RMS	Correlation	*p*-Value
Shrugging	Wrist	−0.003	0.006	0.007	0.98	0.63
	Elbow	−0.004	0.006	0.005	0.98	0.43
	Shoulder	−0.002	0.005	0.004	0.96	0.46

vidual activity classification, e.g. sitting, standing and lying. Since binary decisions were made in terms of discrimination between two activities, the posture threshold method is applicable in these situations. However, this method cannot be used in the case of continuous movements of the upper limb due to unknown thresholds and higher degrees of freedom of the arm motion. Gyroscopes have been used to improve accuracy of the estimates by accelerometers [9]. Although this reported data fusion works in specific circumstances, e.g. standing and sitting, it will need more accelerometers and gyroscopes than our system in order to locate the whole arm in space. This will add more costs to the designed system.

The effectiveness of our motion detector has been demonstrated by comparing its outcomes to the ground-truth generated by a standard optical motion analysis system. In most circumstances, the proposed motion detector has RMS position errors that are less than 1 cm, and RMS angle errors that are 2.5–4.8°. These results suggest that under the testing circumstance, the proposed motion analysis can reach a high accuracy. In other words, the proposed kinematic model and Lagrangian based optimisation method have been appropriately established for detection of upper arm movements. The experimental results also reveal that, even though the tests only last a few minutes, it clearly shows that no significant drift appears in the estimates of the arm movements. This indicates that the proposed strategy ideally handles the drift problem usually buried in an inertial sensing based implementation. Based on these positive outcomes, in the future work we will study the performance of the proposed system in a longer term.

Nevertheless, this proposed motion tracker failed to accurately detect smaller movements, e.g. less than 0.5 cm or 2°. This outcome is similar to those reported by Luinge [15], where the Kalman filter was used to provide stable orientational estimation. These errors may also be caused by relative movements of sensors (or markers) regarding the underlying bony anatomy [22], incorrect marker placement, joint centre mistaken, etc. [23]. To improve systematic accuracy, we have considered a properly designed sensor attachment in order to produce kinematic data with less noise. This attachment will allow the sensors to be rigidly mounted on the upper limb. It may maximally reduce the relative motion between the sensors and the underlying bones. Moreover, our current system requires the subject to sit down during the movement assessment. A potential solution is to add the lower limb kinematic models to the current model, which is similar to the one for the upper limb. In due course, we may release the subject's mobility constraint.

Donning and doffing of this motion sensor system has not been formally addressed in this paper. However, it has been recognized that the accuracy of measurements and cooperation of patients fully relies on this factor if the system is used at home. Furthermore, to allow a physiotherapist to observe the motion samples performed by patients, a touch screen based platform is being designed. This configuration is similar to that shown in Fig. 1 but the graphic interface is still under development.

5. Conclusion

An upper limb motion tracking system with two commercial inertial sensors has been presented in this paper. A kinematic model of the arm allows the wrist and elbow joints to be located. In order to estimate the shoulder position, a Lagrangian based optimisation method was then adopted, integrating the translation and rotation components of the wearable inertial sensors. We then evaluated the performance of the proposed motion detector which measures the position of the upper limb during movements. The results were very promising, indicating that the proposed motion detector could be integrated into a home based rehabilitation system to report the upper limb movements of a patient.

In future work, we intend to improve the sensor attachment and also generate a more comprehensive human motion model that describes the movements of human lower and upper limbs.

Acknowledgements

This is a part of SMART Rehabilitation Project funded by the UK EPSRC under Grant GR/S29089/01. The authors thank Dr. J. Hammerton for generating Fig. 1. We also acknowledge Charnwood Dynamics Ltd. for providing a CODA motion tracking system for system evaluation.

References

[1] Wade D, de Jong B. Recent advances in rehabilitation. Br Med J 2000;320:1385–8.
[2] Cauraugh J, Kim S. Two coupled motor recovery protocols are better than one electromyogram-triggered neuromuscular stimulation and bilateral movements. Stroke 2002;33:1589–94.
[3] Burdea G, Popescu V, Hentz V, Colbert K. Virtual reality-based orthopedic telerehabilitation. IEEE Trans Rehabil Eng 2000;8(3): 430–2.
[4] Edgeton V, Kim S, Ichiyama R, Gerasimenko Y, Roy R. Rehabilitative therapies after spinal cord injury. J Neurotraum 2006;23:560–70.
[5] Reinkensmeyer D, Dewald J, Rymer W. Robotic devices for physical rehabilitation of stroke patients: fundamental requirements, target therapeutic techniques, and preliminary designs. Technol Disabil 1999;5:205–15.
[6] van Exel N, Koopmanschap M, Scholte op Reimer W, Niessen L, Hujisman R. Cost-effectiveness of integrated stroke services. Q J Med 2005;98:415–25.
[7] Saunders J, Inman V, Eberhart H. The major determinants in normal and pathological gait. J Bone Joint Surg 1953;35A:543–58.
[8] Veltink P, Bussmann H, de Vries W, Martens W, van Lummel R. Detection of static and dynamic activitties using uniaxial accelerometers. IEEE Trans Rehabil Eng 1996;4:375–85.
[9] Boonstra M, van der Slikke R, Keijsers N, van Lummel R, de Waal Malefijt M, Verdonschot N. The accuracy of measuring the kinematics of rising from a chair with accelerometers and gyroscopes. J Biomech 2006;39:354–8.

[10] Lyons G, Culhane K, Hilton D, Grace P, Lyons D. A description of an accelerometer-based mobility monitoring technique. Med Eng Phys 2005;27:497–504.
[11] Mayagoitia R, Nene A, Veltink P. Accelerometer and rate gyroscope measurement of the kinematics: an inexpensive alternative to optical motion analysis systems. J Biomech 2002;35:537–42.
[12] Najafi B, Aminian K, Paraschiv-Ionescu A, Loew F, Bula C, Robert P. Ambulatory system for human motion analysis using a kinematic sensor: monitoring of daily physical activity in the elderly. IEEE Trans Biomed Eng 2003;50:711–23.
[13] Krebs H, Volpe B, Aisen M, Hogan N. Increasing productivity and quality of care: robot-aided nero-rehabilitation. J Rehabil Res Dev 2000;37:639–52.
[14] Barbour N, Schmidt G. Inertial sensor technology trends. IEEE Sensors J 2001;1:332–9.
[15] Luinge H. Inertial sensing of human movement. PhD thesis. The Netherlands: Twente University; 2002.
[16] Islam N, Harris N, Eccleston C. Does technology have a role to play in assisting therapy in a care or home environment? A review of practical issues for health practitioners. Quality in Aging, vol. 7, no. 1, 2006.
[17] Bachmann E, McGhee R, Yun X, Zyda M. Inertial and magnetic posture tracking for inserting humans into networked virtual environments. In: Proceedings of the ACM symposium on virtual reality software and technology. 2001;9–16.
[18] Craig J. Introduction to robotics: mechanics and control. NJ: Pearson Prentice Hall; 2005.
[19] Cuthbert D, Wood F. Fitting Equations to data: computer analysis of multifactor data. New York: Wiley; 1980.
[20] Zhou H, Hu H, Hammerton J, Harris N. Applications of wearable inertial sensors in estimation of upper limb movements. Biomed Signal Process Control 2006;1:22–32.
[21] Uiterwaal M, Glerum E, Busser H, van Lummel R. Ambulatory monitoring of physical activity in working situations: a validation study. J Med Eng Technol 1998;22:168–72.
[22] Hingtgen B, McGuire J, Wang M, Harris G. An upper extremity kinematic model for evaluation of hemiparetic stroke. J Biomech 2006;39:681–8.
[23] Anglin C, Wyss U. Review of arm motion analysis. Proc Inst Mech Eng 2000;214:541–55.